JOURNAL OF CHEMICAL INFORMATION AND MODELING

Article

pubs.acs.org/jcim

Binding Kinetics versus Affinities in BRD4 Inhibition

Ming Kuang,[†,‡] Jingwei Zhou,[‡] Laiyou Wang,[†] Zhihong Liu,[‡] Jiao Guo,[*,†] and Ruibo Wu[*,‡]

[†]Guangdong Metabolic Diseases Research Center of Integrated Chinese and Western Medicine, Guangdong TCM Key Laboratory against Metabolic Diseases, Institute of Chinese Medical Sciences, Guangdong Pharmaceutical University, Guangzhou 510006, P. R. China

[‡]School of Pharmaceutical Sciences, Sun Yat-sen University, Guangzhou 510006, P. R. China

Supporting Information

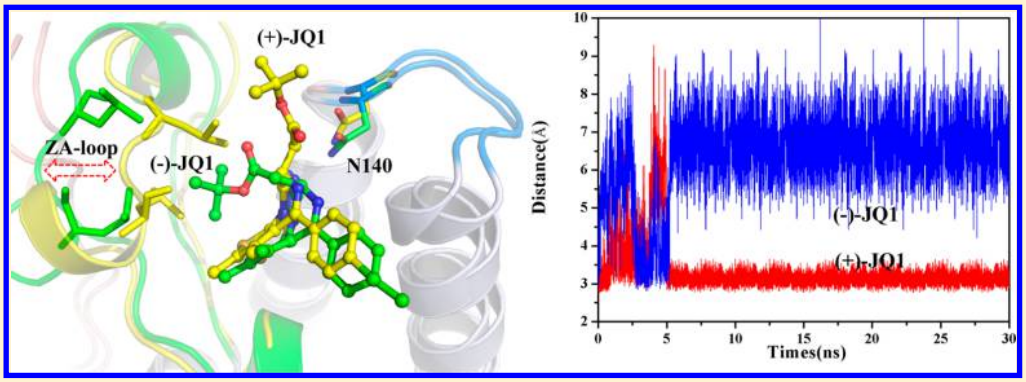

ABSTRACT: Bromodomains (BRDs) are protein modules that selectively recognize histones as a "reader" by binding to an acetylated lysine substrate. The human BRD4 has emerged as a promising drug target for a number of disease pathways, and several potent BRD inhibitors have been discovered experimentally recently. However, the detailed inhibition mechanism especially for the inhibitor binding kinetics is not clear. Herein, by employing classical molecular dynamics (MD) and state-of-the-art density functional QM/MM MD simulations, the dynamic characteristics of ZA-loop in BRD4 are revealed. And then the correlation between binding pocket size and ZA-loop motion is elucidated. Moreover, our simulations found that the compound (−)-JQ1 could be accommodated reasonably in thermodynamics whereas it is infeasible in binding kinetics against BRD4. Its racemate (+)-JQ1 proved to be both thermodynamically reasonable and kinetically achievable against BRD4, which could explain the previous experimental results that (+)-JQ1 shows a high inhibitory effect toward BRD4 (IC_{50} is 77 nM) while (−)-JQ1 is inactive (>10 μM). Furthermore, the L92/L94/Y97 in the ZA-loop and Asn140 in the BC-loop are identified to be critical residues in (+)-JQ1 binding/releasing kinetics. All these findings shed light on further selective inhibitor design toward BRD family, by exploiting the non-negligible ligand binding kinetics features and flexible ZA-loop motions of BRD, instead of only the static ligand−protein binding affinity.

INTRODUCTION

Epigenetic regulation of gene expression is currently the focus of intensive research in the postgenomic era.[1−5] Histones are subjected to a range of post-translational modifications.[1,6] The histone modifications, usually namely "histone code",[7] are found mainly on the N-terminal histone tails that protrude from the globular core of the nucleosome and include acetylation, methylation, phosphorylation, ribosylation, biotinylation, citruillination, and SUMOylation.[1,8] Each modification can affect the chromatin structure, but the overall state of chromatin is ultimately determined by combinations of these modifications.[9] "Readers" of epigenetic marks, which recognize covalent modifications of histone proteins or DNA, are structurally diverse proteins each containing one or more evolutionarily conserved effector modules.[10−13] Among the "Readers", bromodomains (BRDs), which are protein modules containing approximately 110 amino acids and including a left-handed four-helix bundle (αZ, αA, αB, αC) as well as the varying loop regions (ZA and BC, as shown in Figure 1), are the only interaction modules that specifically recognize acetylated lysine residues of histones during transcriptional activation.[14−18] Many of BRDs are regulators of gene transcription such as histone acetyltransferases, components of chromatin remodeling complexes, and methyltransferases.[16,19] Human proteome analysis has revealed that there are eight distinct BRD families, representing 61 different BRDs from 46 separate proteins, although others may still be undiscovered.[11,16]

The bromodomain and extra terminal (BET, belong to family II BRDs) include BRD2, BRD3, BRD4, and BRDT, and they exhibit a high level of sequence conservation.[20−22] The BRD4 has emerged as a promising drug target for a number of disease pathways that are characterized by changing the

Received: May 10, 2015
Published: August 11, 2015

DOI: 10.1021/acs.jcim.5b00265
J. Chem. Inf. Model. 2015, 55, 1926−1935

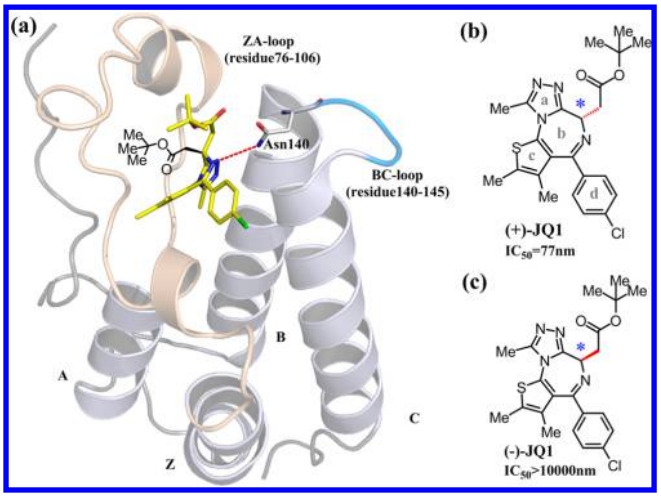

Figure 1. (a) Ribbon illustration of the crystal structure of BRD4 complex with (+)-JQ1 (PDB code 3MXF). The four α-helices and two important loops (ZA-loop and BC-loop, around binding site) are marked. (b,c) Chemical structures and IC_{50} values of (+)-JQ1 and (−)-JQ1 inhibitors (chiral atoms are highlighted by blue asterisk). The yellow stick structure indicates the (+)-JQ1 in crystal structure, and the red solid/dashed wedge lines indicate the different orientation of (−)-JQ1 in BRD4. Asn140 is a conserved residue in BRDs and forms a strong hydrogen bond with JQ1 ligands.

epigenetic cell signature.[23−25] Recently, Filippakopoulos et al.[23] have identified a highly potent methyltriazolodiazepine-like inhibitor of BRDs, (+)-JQ1, which has very high affinity with an IC_{50} value of 77 nM for BRD4, but the (−)-JQ1 stereoisomer is inactive against BRD4 with the IC_{50} value above 10 000 nM, as shown in Figure 1. Meanwhile, it has been proposed that the plasticity and accessibility of the acetyl-lysine binding site to accommodate diverse inhibitors are likely due to the flexible ZA-loop.[23,26] However, the detailed loop motion and its functional roles are still not clear. Herein, by employing molecular dynamics (MD) simulations on BRD4 with explicit solvent at the molecular mechanics or hybrid quantum mechanical/molecular mechanical (QM/MM) level, we have identified the exact optimal binding modes of the two racemates ((+)-JQ1 and (−)-JQ1) and revealed the flexibility of the ZA-loop in BRD4. Meanwhile, we illuminate the relationship between pocket size and ZA-loop motion, which is induced by the ligands. Furthermore, the functional roles of the ZA-loop in regulating the binding affinity with JQ1 and mechanism details on the releasing/binding kinetics of (+)-JQ1 are elucidated. All of these findings are guidable for selective inhibitor design toward BET family.

METHODS

1. Classical MM MD Simulations. The electroneutral enzyme−ligand complex was built from the crystal structure of BRD4 binding with (+)-JQ1 (PDB: 3MXF).[23] The ff99SB force field[27] and GAFF force field[28] were employed for the proteins and the two JQ1 ligands, respectively. The partial atomic charges of these small molecule ligands were fitted from the restrained electrostatic potential (RESP)[29] charge at HF/6-31G* theoretical level by using the Gaussian09 package.[30] The key charge parameters of JQ1 compounds were provided in Table S1, and their surrounding active site environment was represented in Figure S1. The amino acid side chain protonation states were assigned using default AMBER protonation states, and the protonation states of the key residues in BRD4 were also checked manually. His71 was protonated at the epsilon position to form hydrogen bonds with the water molecule nearby. And then the whole system was solvated within a cubic box of TIP3P water molecules[31] by extending 8 Å from the BRD4 protein surface. Finally, the initial coordinates and topology files were generated by the *tleap* program in AMBER12.[32]

Before the heating MD simulation, the system was optimized by three steps. First, the water molecules were minimized while keeping the protein and substrates constrained. Then, the side chains of the protein were relaxed while keeping the main chain restrained. Finally, the entire system was optimized. For each minimization step, the conjugate gradient iterations were carried out for 2000 cycles after performing 2000 steps steepest descent energy minimization. After the optimization, the system was heated up from 0 to 310 K gradually under the NVT ensemble for 50 ps. Then, 50 ps MD simulations were performed under the NPT ensemble to relax the system density to about 1.0 g/cm^3, with the target temperature of 310 K and the target pressure of 1.0 atm. The Berendsen thermostat method[33] was used to control the system temperature. Finally, 100 ns MD simulation under the NVT ensemble was carried out via employing the periodic boundary condition. The SHAKE algorithm[34] was applied to constrain all hydrogen-containing bonds with a tolerance of 10^{-5} during the MD simulations. A cutoff of 12 Å was set for both van der Waals and electrostatic interactions. All the simulations were accomplished in AMBER12.[32]

To characterize the dynamics of the ZA-loop during the ligand releasing process, the umbrella sampling technique[35] was employed to effectively capture all conformations along the ligand releasing pathway. The distance between MET107:Cα and (+)-JQ1:C13 (see Figure S1) atoms was chosen as the reaction coordinate (RC). The MD simulations were performed with a series of biasing harmonic potential (10−25 kcal/mol) along the RC from 13.0 to 30.0 Å (there was total of about 56 simulation windows, and each window was separated by 0.3 Å). The equilibrium structure from the most nearby window was employed to be the initial structure for the next window. At least 20 ns MD simulations were carried out to check if it became stable for each window, via monitoring the RMSD values. And then additional 15 ns productive MD simulations were performed for sampling. Finally, the collected RC data (the last 10 ns MD trajectory for each window) were analyzed by the weighted histogram analysis method (WHAM)[36] to generate the potential of mean force (PMF) (namely free energy profile).

Cluster analysis is a general unsupervised technique for finding patterns within data.[37−39] In this work, the root mean-square deviation (RMSD)-based clustering was performed with *ptraj*, a simulation analysis tools implemented in AMBER12. As one of the most popular clustering algorithms, the average linkage cluster algorithm was used herein.[40] Each cluster contained a representative structure whose RMSD was equidistant to all other cluster members. Structures were collected by sampling at 200 ps intervals, and cluster analysis was based on the heavy atoms of BRD4 protein to generate a sum of five clusters (only two clusters were kept). The volumes of the substrate binding pocket were measured using POVME, an algorithm for measuring pocket volume.[41] Structures were collected by sampling at 50 ps intervals and aligned to the initial crystal structure (PDB: 3MXF). An inclusion sphere with a

DOI: 10.1021/acs.jcim.5b00265
J. Chem. Inf. Model. 2015, 55, 1926−1935

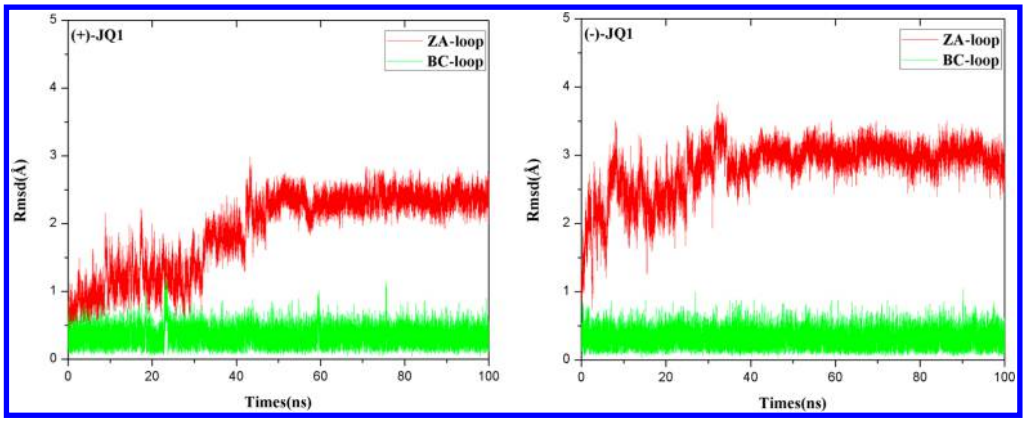

Figure 2. Time series of the skeleton-atoms RMSD for the two loops in BRD4.

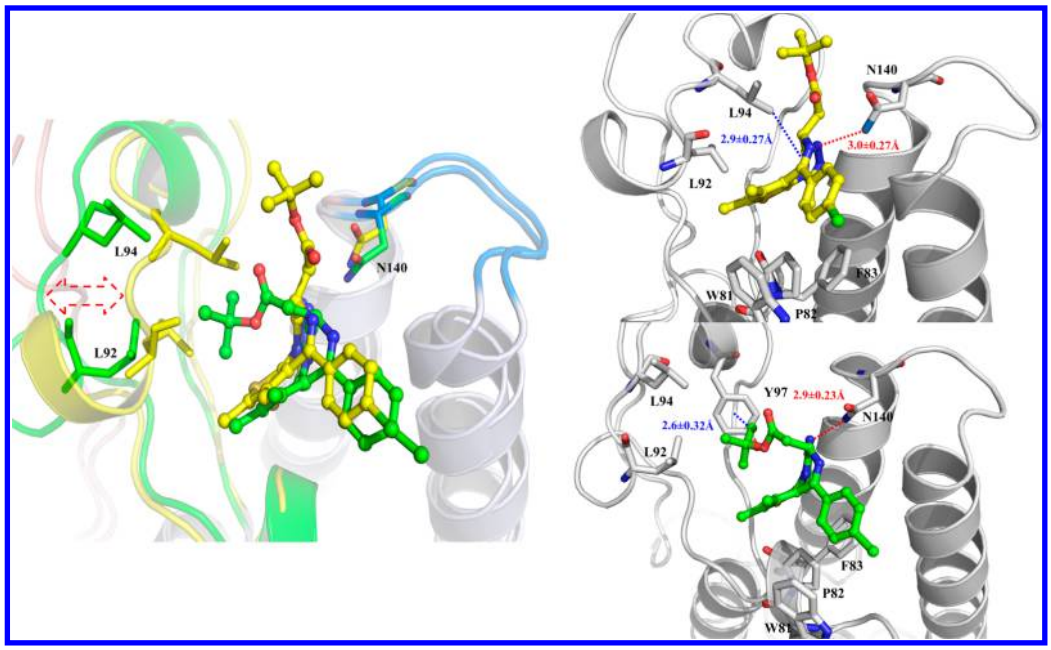

Figure 3. Comparison of the ligand binding modes with key residues in ZA-loop (yellow one for (+)-JQ1 and green one for (−)-JQ1). The left side image is the structural overlap, and the red double-head arrow indicates the distinguishable motion of ZA-loop; the detailed distance evolution between the two loops (namely between Asn140:Cα and Leu94/Leu92:Cα) is shown in Figure S3. The two distinct $\sigma-\pi$ interactions are highlighted in red in the right side of the image (the distances between the carbon atom and the center of aromatic ring are noted).

radius of 12 Å was defined that entirely encompassed the binding pocket. A written shell script was used to automatically calculate the volumes of all collected structures automatically. And all molecular figures shown in this article were created using PyMOL.[42]

2. Born−Oppenheimer *ab Initio* QM/MM MD Simulations. The equilibrium enzyme−ligand complex systems from the above MD simulations were cut into a sphere by removing the solvent water molecules beyond 30 Å of the C22 atom (as shown in Figure S1) of (+)-JQ1/(−)-JQ1. The resulting systems were then partitioned into QM and MM subsystems. The Asn140 and ligands were chosen as the QM subsystem (~65 atoms in total), which was treated by B3LYP[43,44] with the 6-31G* basis set. The QM/MM boundaries were described by the pseudobond approach with improved pseudobond parameters.[45−48] All the remaining atoms were described by the same MM force field used in the previous classical MD simulations. For all QM/MM calculations, the spherical boundary condition[45,48] was applied, and atoms more than 22 Å away from the center were fixed. Cutoffs of 18 and 12 Å were employed for the electrostatic and van der Waals interactions, respectively. There was no cutoff for the electrostatic interactions between QM and MM regions. After minimization of the prepared QM/MM systems, 25 ps QM/MM MD simulations were performed using a time step of 1 fs and the Beeman algorithm[49] to integrate the Newton equations of motion. The Berendsen thermostat method[33] was used to control the system temperature at 310 K. The configurations of the last 5 ps were collected for data analysis. All *ab initio* QM/MM calculations were performed in modified QChem-Tinker programs.[50,51] A similar QM/MM modeling protocol had been extensively employed in our previous studies.[52−55]

RESULTS AND DISCUSSION

1. Static Ligand Binding Modes of JQ1. To probe the structural stability of the BRD4-JQ1 complex, the detailed RMSD evolution along the 100 ns MM MD simulations are

DOI: 10.1021/acs.jcim.5b00265
J. Chem. Inf. Model. 2015, 55, 1926−1935

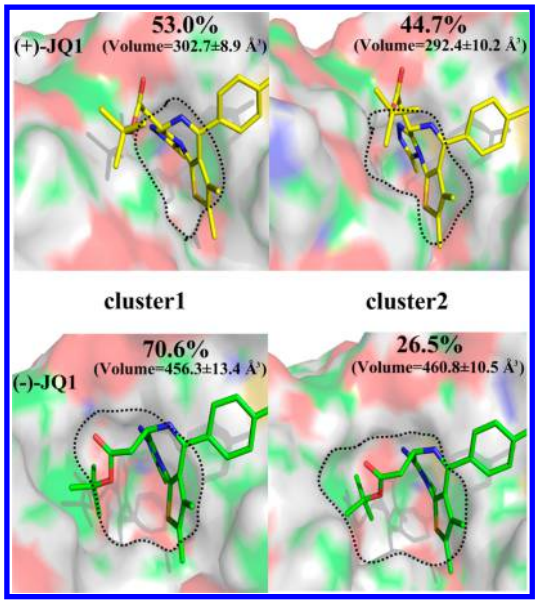

Figure 4. Pocket surface illustration for two racemates of JQ1 binding to BRD4 based on cluster analysis. The model binding with (+)-JQ1 is left-rotated to make the pocket mouth directly face toward us for clear observation.

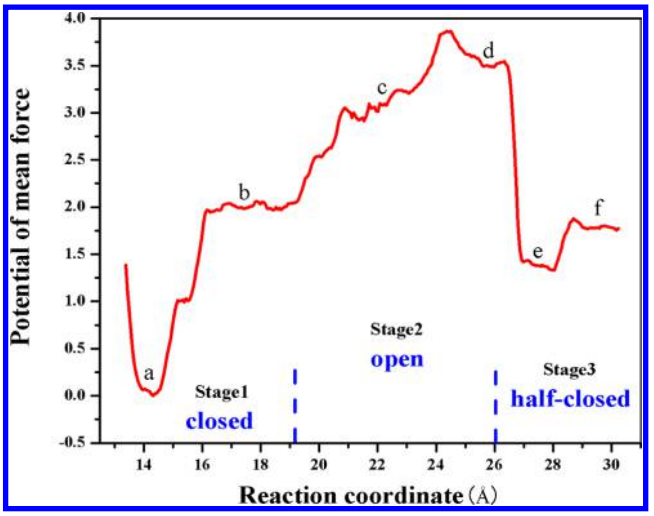

Figure 6. Free energy profiles of (+)-JQ1 releasing along the defined reaction coordinate. The representative structures at the selected points (a/b/c/d/e/f) are shown in Figure 7. The benchmark test on the convergence of PMF curve is provided in Figures S9 and S10.

summarized in Figure S2. It indicates that the BRD4 protein structures are very stable with the backbone RMSD value near 2 Å after 40 ns MD simulations, and most fluctuations are due to the loops. Further RMSD comparisons (see Figure 2) indicate that the BC-loop is as stable as observed in *apo*-BRD4 (see Figure S2). However, the ZA-loop is very flexible (from 0.5 to 2.5 Å) to achieve the final optimal binding modes of (+)-JQ1. Since the RMSD of the ZA-loop is also around 2.5 Å in the stable *apo*-state (see Figure S2), we proposed that ligand-induced conformation change is unnecessary for the active inhibitor (+)-JQ1 binding to the active pocket (will be discussed again in section 2). Regarding the inactive inhibitor (−)-JQ1, as its RMSD is near 3 Å (see Figure 2) which is bigger than that in the *apo*- BRD4, it indicates that ZA-loop motion is required to accommodate the ligand into the binding pocket. That is, the active pocket is extendible (will discuss it *infra*), which had also been proposed in previous studies.[23,26] On the basis of the flat RMSD evolution for the ZA-loop after about 40 ns of simulations, the inactive inhibitor (−)-JQ1

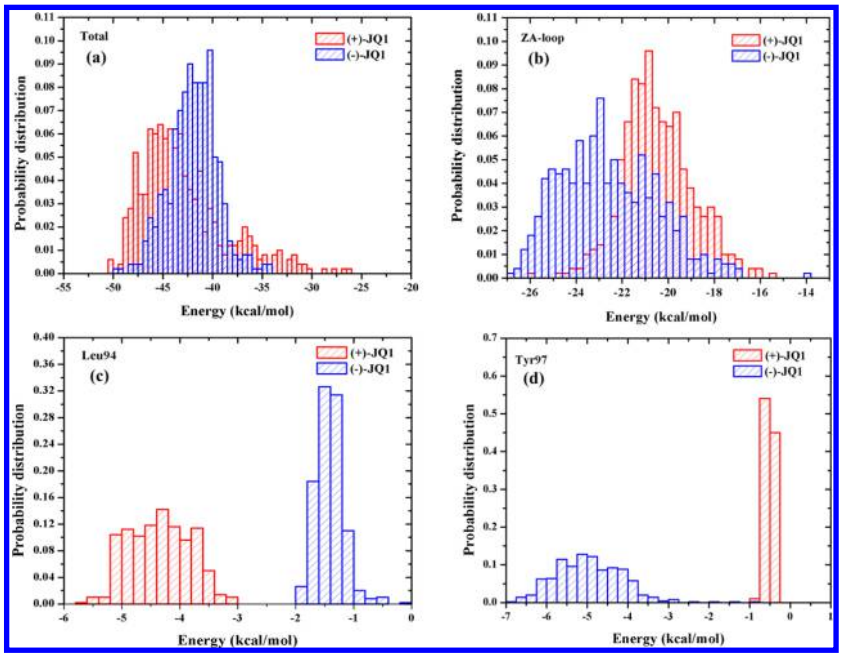

Figure 5. Interaction energy analysis between selected residues and ligand. (a) The total stabilization energy from the protein environment for (+)-JQ1 and (−)-JQ1 ligands. (b) The interaction energy between ZA-loop and the two racemates. (c) The interaction energy between the L94 and the two racemates. (d) The interaction energy between the Y97 and the two racemates. The detailed interaction energy analysis between ZA-loop/BC-loop and ligand are summarized in Figure S5. For the BC-loop, it presents a similar interaction with the two ligands; especially, D144 is disadvantageous while K141 is advantageous in stabilizing the two racemates of JQ1. All interaction energies are calculated based on 5000 snapshots from the equilibrium QM/MM MD trajectories.

DOI: 10.1021/acs.jcim.5b00265
J. Chem. Inf. Model. 2015, 55, 1926−1935

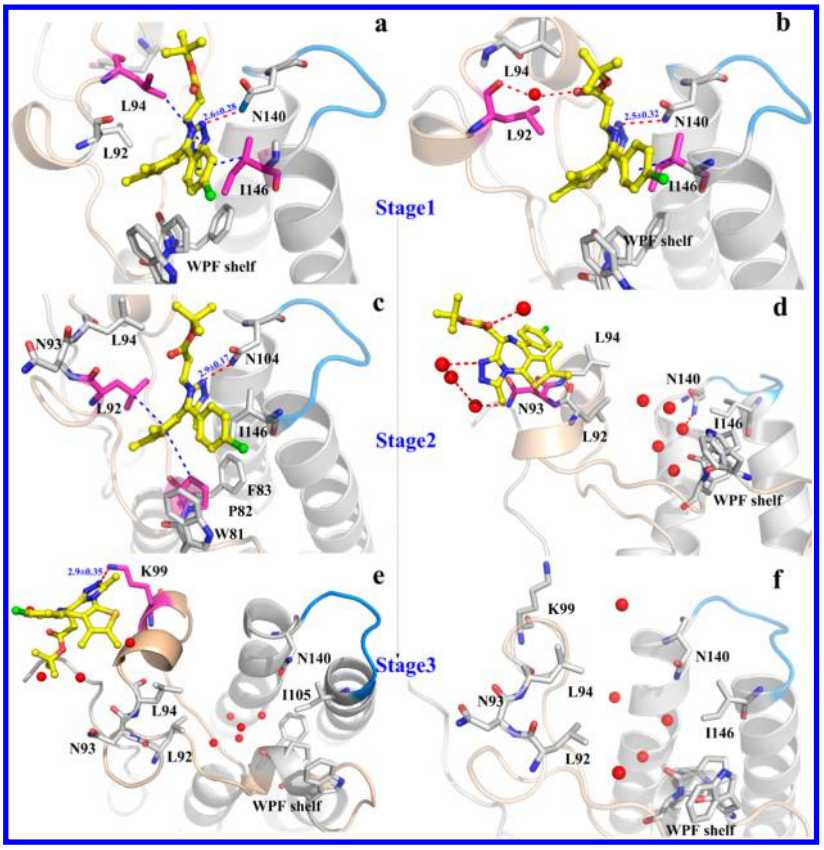

Figure 7. Representative structures in the release process of (+)-JQ1 from BRD4. (a,b) represent the first stage, (c,d) show the second stage, and (e,f) reveal the third stage. The detailed location of (a−f) along the release process is referred to Figure 6. The residues playing key roles in ligand releasing are highlighted in purple, and most water molecules in the pocket are shown in a red ball. The key hydrogen bonds are shown in a red-dashed line, and π-stacking interaction is noted by a blue-dashed line. BC-loop is colored in blue, and ZA-loop is colored in wheat.

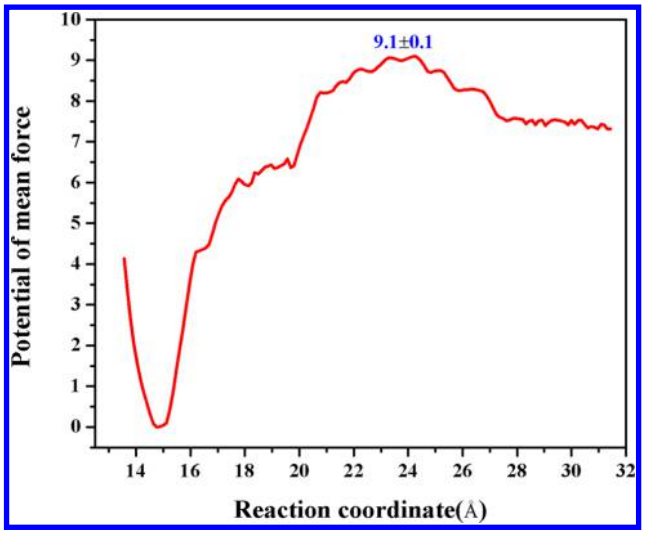

Figure 8. Free energy profiles of (−)-JQ1 releasing along the defined reaction coordinate. The standard deviation (0.1 kcal/mol) is estimated with the same methods shown in Figure S9.

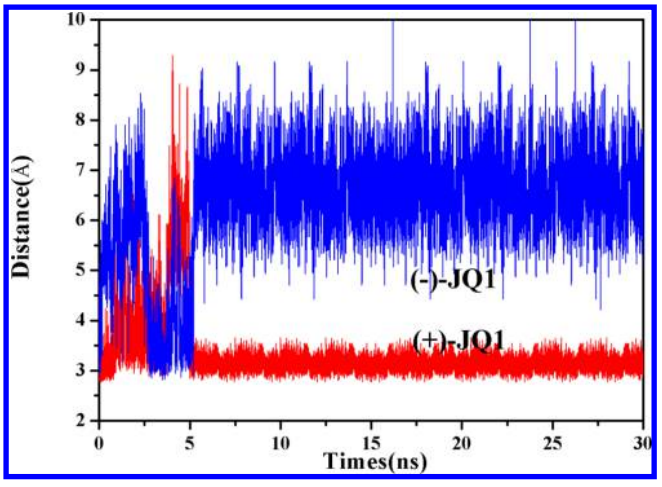

Figure 9. Representative distance evolution between Asn140:N and JQ1:N (the strong hydrogen bond (HB) heavy-atom between N140 and JQ1; see Figure S1.). Another three representative spontaneously binding trajectories for (+)-JQ1 and (−)-JQ1 are summarized in Figure S8. The (−)-JQ1 would form a hydrogen bond with Asn140 during the simulated annealing (SA) process (~2.5−5 ns in this case). However, it would be lost at the end of the SA procedure (~5−8 ns) and would not reconstruct the hydrogen bond interaction during the productive MD simulations (8 ns later). Moreover, (−)-JQ1 might move backward into the solvent again as observed in some cases as presented in Figure S8.

would be also well accommodated in BRD4; thus, it is interesting to answer how the ZA-loop motion occurs when (−)-JQ1 instead of (+)-JQ1 binds to active site.

As shown in Figure 3, the structural superposition clearly reveals that the BC-loop as well as the strong hydrogen bond with the ligand are very stable for either (+)-JQ1 or (−)-JQ1. Moreover, the side group on the chiral center of (+)-JQ1 locates at the free space between two loops and toward the solvent outside the pocket, which matches well to the original

DOI: 10.1021/acs.jcim.5b00265
J. Chem. Inf. Model. 2015, 55, 1926−1935

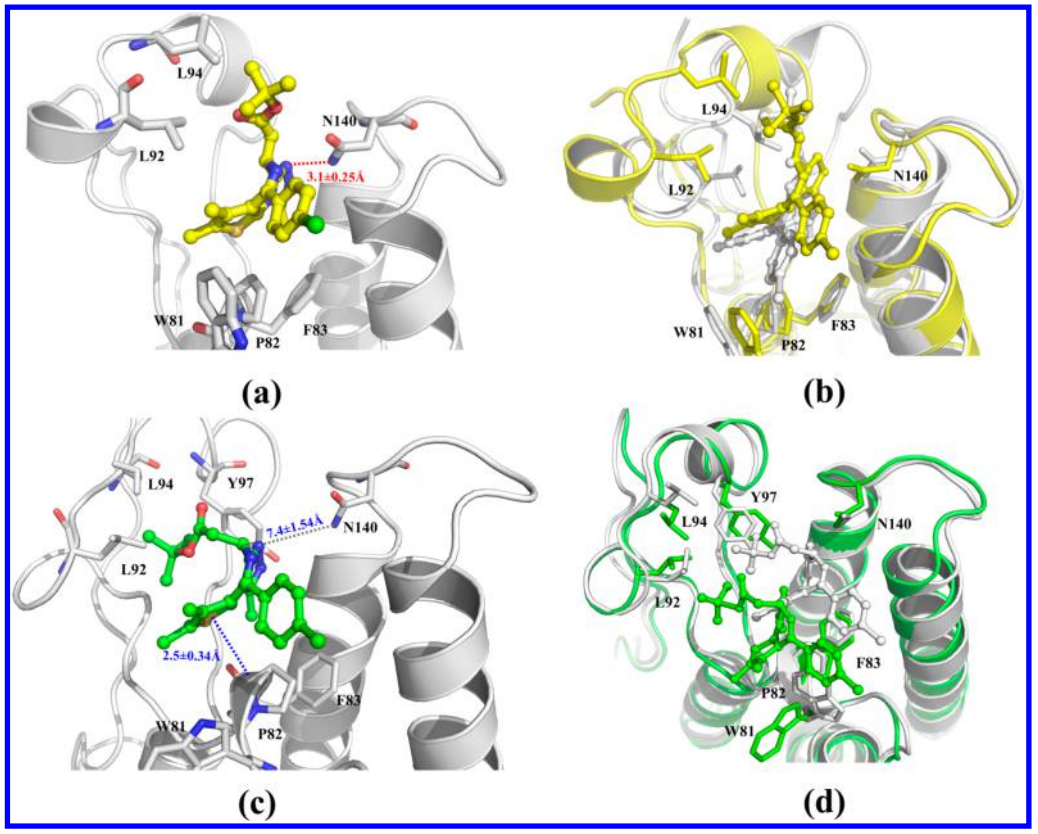

Figure 10. Representative binding modes of (+)-JQ1 and (−)-JQ1 (yellow one for (+)-JQ1 (a) and green one for (−)-JQ1 (c)) at the equilibrium state from the spontaneously binding trajectories (refer to Figure 9), and the corresponding structural superposition referring to the optimal binding models (in gray) mentioned in Figure 3 ((b) for (+)-JQ1 and (d) for (−)-JQ1 respectively).

binding modes in XRD (X-ray diffraction) structure (PDB: 3MXF); thus, it shares a similar RMSD for the ZA-loop in *apo*-BRD4 as mentioned above. In contrast, the ZA-loop is pushed out since the side group on the chiral center of (−)-JQ1 is orientated to the inside of the binding pocket and it would occupy the original location for L94 and L92 in the ZA-loop, and thus brings a bigger RMSD of the ZA-loop as presented in Figure 2. As a result, the binding modes are different between the two racemates (see Figure 3) and the stable $\sigma-\pi$ interaction is observed between L94 and the a-ring of (+)-JQ1, while it is destroyed and replaced by another $\sigma-\pi$ interaction between (−)-JQ1 and the aromatic ring of Y97. Obviously, the Y97 will flip over from outside to inside pocket as the ZA-loop is pushed out by (−)-JQ1. In sum, the most significant difference is that the side chain on the chiral center is anchored by L94 and N140 for (+)-JQ1 whereas it is restricted by Y97 and N140 for (−)-JQ1 in the final optimal binding modes.

As distinguished ZA-loop motion is required upon (−)-JQ1 binding to BRD4, with enlargement of the binding pocket to accommodate it, further cluster analysis and pocket volumes calculation are performed to investigate the expansion of the binding pocket. As shown in Figure 4, the volume of the active pocket is larger than 456 Å^3 upon (−)-JQ1 binding to BRD4, while that is only about 298 Å^3 for (+)-JQ1. Obviously, the pocket mouth is bigger for (−)-JQ1 than for (+)-JQ1 binding into BRD4, which is consistent with the bigger distance between the two loops, as shown in Figure 3. Regarding to the *apo*-BRD4, the computationally predicted pocket volume is about 283.6 ± 5.7 Å^3, which is close to that for the (+)-JQ1 binding BRD4. It indicates that the active pocket opening is essential for binding with (−)-JQ1 whereas not necessary for (+)-JQ1. Foreseeably, much more water would enter into the active pocket if (−)-JQ1 binding into BRD4 included a bigger pocket mouth (see Figure S4). As a result, the ligand binding environment will be totally different since the dielectric constant of the binding pocket would be modulated by the number of water molecules in the binding pocket, leading to a different binding affinity.

Therefore, to reveal the functional roles of the ZA-loop in binding JQ1, the state-of-the-art density functional QM/MM MD simulations were further performed to accurately analyze the protein−ligand interaction energy, as summarized in Figures 5 and S5. The total binding affinity (namely stabilization energy contributed from protein environment) is about −45 kcal/mol for (+)-JQ1, similar to that for (−)-JQ1 (−42 kcal/mol; see Figure 5a); thus, (−)-JQ1 would also have a high binding affinity in BRD4. Similarly, as shown in Figure 5b, the interaction energy between (−)-JQ1 and the ZA-loop (−23 kcal/mol) is higher than that for (+)-JQ1 (−21 kcal/mol), without distinctive thermodynamics features between the two racemates. The only difference for the two racemates is the stabilization energy contributed from the L94 and Y97; as shown in Figure 5(c, d), L94 is a critical residue to stabilize the (+)-JQ1 (−4 kcal/mol) while Y97 is important in stabilizing the (−)-JQ1 (−5 kcal/mol), which is consistent with the different binding modes as observed in Figure 3.

Experimentally, (−)-JQ1 had been proven to be inactive whereas (+)-JQ1 was active against BRD4.[23] Herein, our modeling indicates that BRD4 could accommodate both of them, as its could enlarge the binding pocket via the ZA-loop motion, which is consistent with the experimental results that several kinds of inhibitor with different skeletons are

DOI: 10.1021/acs.jcim.5b00265
J. Chem. Inf. Model. 2015, 55, 1926−1935

identified.[19,56] Indeed, the ZA-loop is very flexible to optimize the binding modes of the inactive inhibitor (−)-JQ1 and makes it also thermodynamically favorable in comparison to the active inhibitor (+)-JQ1. In this case, it is experimentally and computationally incongruent when seen from a "ligand−protein binding affinity viewpoint". Since the more flexible ZA-loop and bigger pocket volumes are observed for (−)-JQ1 in comparison to (+)-JQ1 upon binding to BRD4, it raises a hypothesis that the inactivity of (−)-JQ1 is due to the facility in the releasing process or the difficulty in binding procedure in kinetics (*vide infra*).

2. Binding/Releasing Kinetics of JQ1. To investigate the dynamic releasing process of ligands, the free energy profiles for (+)-JQ1 releasing from the active pocket are mapped out as shown in Figure 6. It indicates that the release of (+)-JQ1 is very facile kinetically, with a less than 4 kcal/mol barrier, and involving three stages (see Figures 6 and 7). At the beginning of the first stage (see Figure 7a), the strong hydrogen bond (HB) between N140 and (+)-JQ1 is maintained well, keeping ∼2.6 Å between the two HB heavy atoms. And the above-mentioned $\sigma-\pi$ stacking interaction {Leu 94:CD1--(+)-JQ1: a-ring}, as well as the $\sigma-\pi$ stacking interaction between Ile146:CB and (+)-JQ1: d-ring, is very stable. At the end of the first stage (see Figure 7b), both HB interaction with N140 and $\sigma-\pi$ stacking interaction with Ile146 are maintained well, while the {Leu 94:CD1-- (+)-JQ1: a-ring} $\sigma-\pi$ stacking interaction is destroyed and replaced by HB interaction mediated by a water molecule. During the second stage (see Figure 7c and d), the N140:ligand HB interaction and Ile146—ligand $\sigma-\pi$ stacking interaction were broken. Instead, several water molecules entered into the pocket and surrounded the hydrophilic N140 and Ile146, as well as the polar group of (+)-JQ1, to construct a new hydrogen bond network. At the end of the second stage, namely near the highest barrier region as shown in Figure 6, since the $\sigma-\pi$ stacking interactions with Leu92 and Leu94 were totally damaged, (+)-JQ1 is no longer anchored between the ZA-loop and BC-loop; then molecular hopping occurred, surrounded by several water molecules finally. At the beginning of the third stage (see Figure 7e), (+)-JQ1 is almost away from the active pocket, but is still in contact with Lys99 (in ZA-loop) by a hydrogen bond interaction, thus presenting a flat region (namely local metastable state, point e) in the free energy profile as shown in Figure 6. When this HB is finally destroyed, the ligand is completely solvated in water solution at the end of the third stage (see Figure 7f).

Regarding the binding pocket, it would involve "closed"-"open"-"half-closed" three stages along the releasing process, which is consistent with the conformation change of the ZA-loop, as shown in Figure 7. At the first stage (aand b), the secondary structure of the ZA-loop is stable since the protein−ligand interaction is still very strong and maintained well. At the second stage, followed by the breakage of the strong hydrogen bond between N140 and the ligand, the ZA-loop moves forward to the outside solvent and enlarges the binding pocket as well as increases the water molecules in the active site. At the third stage, as the ligand is finally released from the binding pocket, all of the interactions between the ZA-loop and ligand are lost. From then on, the enzyme will recover to the *apo*-state spontaneously; thus, the ZA-loop moves inwardly and shrinks the binding pocket with extrusion of many water molecules. As shown in Figure S6, the water number evolution, as well as the distance evolution between secondary-structure-stable BC-loop and conformation-flexible ZA-loop along the ligand releasing, is highly consistent with the observed "closed"-"open"-"half-closed" kinetics. At the second stage, it is required to destroy the very strong HB interaction with N140 as well as the important $\sigma-\pi$ stacking interaction with ZA-loop, which brings the most hindering effect; thus, it is the kinetically advantageous stage for preventing (+)-JQ1 releasing, to increase the so-called "drug-target" resident time. Intriguingly, a higher-energy-barrier "second stage" and unstable "third stage" are identified for (−)-JQ1, as shown in Figure 8. Therefore, the release of (−)-JQ1 is not as facile as the (+)-JQ1 release from the pocket.

For the binding kinetics procedures, considering the bigger active pocket is essential to nestle the (−)-JQ1, as observed in Figure 4, the ligand-induced ZA-loop conformation change is required to open the pocket as we mentioned in section 1. Our further steered molecular dynamics (SMD) and simulated annealing(SA)/productive MD simulations (see detailed computational protocol in Figure S7) enabled observation of the binding kinetics difference between (+)-JQ1 and (−)-JQ1. A total of 20 independent MD trajectories for (+)-JQ1 and (−)-JQ1 are obtained respectively, and the distance between JQ1 and Asn140 which represents the strong hydrogen bond between BRD4 and JQ1 (highlighted in red dashed line in Figures 3 and S1) is selected to detect whether (+)-JQ1/(−)-JQ1 ligands bind to the active site. It is found that (+)-JQ1 would successfully enter into the binding sites four times during the simulated annealing process spontaneously and would not immigrate backward into the solvent anymore, whereas (−)-JQ1 could not enter into the binding sites even if the ligand had been steered to the mouth of the active site, as shown in Figure 9 (see more details in Figure S8). It reveals that (+)-JQ1 is facile to binding into the pocket, which leads to its achievable binding kinetics and consistency with its good inhibitory effect (∼77 nM). In contrast, (−)-JQ1 experiences difficulty in entering into the binding site and leads to a worse inhibitory effect as experiments showed (>10 000 nM).

To determine the key regulatory factors on the binding kinetics difference between (+)-JQ1 and (−)-JQ1, further structural analysis was summarized in Figure 10. The weak interaction between (+)-JQ1 and Y94 is not observed in the 30 ns SA and productive MD simulation (see Figure 10a). However, the very stable hydrogen bond with the conserved Asn140 residue is formed spontaneously and maintained well (see Figure 10a), which is as strong as observed in the XRD structure and the above-mentioned MD simulations as shown in Figure 3, which share highly similar binding modes (see Figure 10b). In contrast, the significantly important conserved hydrogen bond interaction between the ligand and Asn140 is totally lost. Meanwhile, instead of the π-stacking interaction with Y97, (−)-JQ1 would maintain very stable π-stacking with P82 and locate close to the ZA-loop. The (−)-JQ1 could partially enter into the active pocket to remain at a metastable binding state (see Figure 10c) in the enlarged pocket due to ZA-loop motion. Nevertheless, the binding modes (see Figure 10d) are indeed different from the above-mentioned thermodynamically favorable state as shown in Figure 3. And the escapement of (−)-JQ1 from the active pocket mouth to the solvent could be observed in several MD trajectories (one example in Figure S8). That is, it is kinetically unfavorable to achieve the more stable binding modes due to the lack of a conserved hydrogen bond interaction with Asn140 to further pull the ligand entering into the bottom of the active pocket site. Therefore, we conclude that Asn140 is a critical factor not

DOI: 10.1021/acs.jcim.5b00265
J. Chem. Inf. Model. 2015, 55, 1926−1935

only in "ligand-protein binding affinity" but also in facilitating control along the "inhibitor binding kinetics".

CONCLUSION

By atomic-level MD simulations, the accessibility of the active pocket ranging from fully closed to a completely open state regulated by the ZA-loop in BRD4 is investigated directly. And by further electronic-level Born−Oppenheimer density functional QM/MM MD simulations, the optimal binding modes of inhibitor (+)-JQ1 are identified, and the critical roles of the ZA-loop in stabilizing the ligands are also clarified. It is found that not only the well-known conserved residue Asn140 in the BC-loop but also the newly characterized L92/L94/Y97 residues in the ZA-loop play important functional roles in (+)-JQ1 binding and releasing dynamics. Furthermore, in comparison with the inactive inhibitor (−)-JQ1, (+)-JQ1 is proven to be both thermodynamically reasonable and kinetically achievable toward BRD4, which is consistent with the high inhibitory activity for (+)-JQ1 as observed in previous experiments.[23] In contrast, the failure of (−)-JQ1 to be an effective inhibitor is due to the unfeasible binding kinetics features against BRD4. It is found that Asn140 is not only important in "ligand−protein binding affinity" but also critical in "binding kinetics" for BRD4 inhibition. This work emphasizes that binding kinetics characteristics (including both binding and releasing) should be carefully considered, even more importantly than the thermodynamically binding affinity for future selective inhibitor design toward BRD.[57] The "drug-target" resident time has been emphasized to promote the drug efficacy recently.[56−58] On the basis of our simulations, (+)-JQ1 is easy to bind but also very facile to release from BRD4; thus, even if (+)-JQ1 showed a high inhibitory effect experimentally and the strong binding affinity with BRD4 is confirmed herein computationally, further structural modification to hinder the release of (+)-JQ1 would be very helpful to increase the "drug-target" resident time, as well as guidance for accelerating the other domain-selective inhibitor design among BET family.

ASSOCIATED CONTENT

Supporting Information

The Supporting Information is available free of charge on the ACS Publications website at DOI: 10.1021/acs.jcim.5b00265.

Figures S1−S10 (PDF)

AUTHOR INFORMATION

Corresponding Authors

*E-mail: jiaoguo_gdpu@hotmail.com.

*E-mail: wurb3@mail.sysu.edu.cn.

Notes

The authors declare no competing financial interest.

ACKNOWLEDGMENTS

This work was supported by the National Science Foundation of China (21203257, 21272289) and Pearl River S&T Nova Program of Guangzhou (2014J2200062). We sincerely acknowledge the funding granted from the Department of Education of Guangdong Province supporting the national major cultivation project for integrated medicine against fatty liver disease. We also thank the National Supercomputing Centers in Shenzhen and Guangzhou for providing the computational resources.

REFERENCES

(1) Kouzarides, T. Chromatin Modifications and Their Function. *Cell* **2007**, *128*, 693−705.

(2) Arrowsmith, C. H.; Bountra, C.; Fish, P. V.; Lee, K.; Schapira, M. Epigenetic Protein Families: A New Frontier for Drug Discovery. *Nat. Rev. Drug Discovery* **2012**, *11*, 384−400.

(3) Heightman, T. D. Therapeutic Prospects for Epigenetic Modulation. *Expert Opin. Ther. Targets* **2011**, *15*, 729−740.

(4) Denis, G. V. Bromodomain Coactivators in Cancer, Obesity, Type 2 Diabetes, and Inflammation. *Discovery Med.* **2010**, *10* (55), 489−499.

(5) Sanchez, R.; Zhou, M. M. The Role of Human Bromodomains in Chromatin Biology and Gene Transcription. *Curr. Opin. Drug Disc.* **2009**, *12*, 659−665.

(6) Bannister, A. J.; Kouzarides, T. Regulation of Chromatin by Histone Modifications. *Cell Res.* **2011**, *21*, 381−395.

(7) Rando, O. J. Combinatorial Complexity in Chromatin Structure and Function: Revisiting The Histone Code. *Curr. Opin. Genet. Dev.* **2012**, *22*, 148−155.

(8) Turner, B. M. Reading Signals on The Nucleosome with A New Nomenclature for Modified Histones. *Nat. Struct. Mol. Biol.* **2005**, *12*, 110−112.

(9) Jenuwein, T.; Allis, C. D. Translating The Histone Code. *Science* **2001**, *293*, 1074−1080.

(10) Lorenzen, J. M.; Martino, F.; Thum, T. Epigenetic Modifications In Cardiovascular Disease. *Basic Res. Cardiol.* **2012**, *107*, 1−10.

(11) Arrowsmith, C. H.; Bountra, C.; Fish, P. V.; Lee, K.; Schapira, M. Epigenetic Protein Families: A New Frontier for Drug Discovery. *Nat. Rev. Drug Discovery* **2012**, *11*, 384−400.

(12) Dawson, M. A.; Kouzarides, T. Cancer Epigenetics: From Mechanism to Therapy. *Cell* **2012**, *150*, 12−27.

(13) Chi, P.; Allis, C. D.; Wang, G. G. Covalent Histone Modifications - Miswritten, Misinterpreted and Mis-Erased in Human Cancers. *Nat. Rev. Cancer* **2010**, *10*, 457−469.

(14) Dhalluin, C.; Carlson, J. E.; Zeng, L.; He, C.; Aggarwal, A. K.; Zhou, M. M. Structure and Ligand of A Histone Acetyltransferase Bromodomain. *Nature* **1999**, *399*, 491−496.

(15) Furdas, S. D.; Carlino, L.; Sippl, W.; Jung, M. Inhibition of Bromodomain-Mediated Protein-Protein Interactions as A Novel Therapeutic Strategy. *MedChemComm* **2012**, *3*, 123−134.

(16) Filippakopoulos, P.; Picaud, S.; Mangos, M.; Keates, T.; Lambert, J. P.; Barsyte-Lovejoy, D.; Felletar, I.; Volkmer, R.; Muller, S.; Pawson, T.; Gingras, A. C.; Arrowsmith, C. H.; Knapp, S. Histone Recognition and Large-Scale Structural Analysis of The Human Bromodomain Family. *Cell* **2012**, *149*, 214−231.

(17) Muvva, C.; Singam, E. R. A.; Raman, S. S.; Subramanian, V. Structure-Based Virtual Screening of Novel, High-Affinity BRD4 Inhibitors. *Mol. BioSyst.* **2014**, *10*, 2384−2397.

(18) Zhao, H. T.; Gartenmann, L.; Dong, J.; Spiliotopoulos, D.; Caflisch, A. Discovery of BRD4 Bromodomain Inhibitors by Fragment-Based High-Throughput Docking. *Bioorg. Med. Chem. Lett.* **2014**, *24*, 2493−2496.

(19) Hewings, D. S.; Rooney, T. P. C.; Jennings, L. E.; Hay, D. A.; Schofield, C. J.; Brennan, P. E.; Knapp, S.; Conway, S. J. Progress in The Development and Application of Small Molecule Inhibitors of Bromodomain-Acetyl-Lysine Interactions. *J. Med. Chem.* **2012**, *55*, 9393−9413.

(20) Muller, S.; Filippakopoulos, P.; Knapp, S. Bromodomains as Therapeutic Targets. *Expert Rev. Mol. Med.* **2011**, *13*, 1−21.

(21) Dawson, M. A.; Prinjha, R. K.; Dittmann, A.; Giotopoulos, G.; Bantscheff, M.; Chan, W. I.; Robson, S. C.; Chung, C. W.; Hopf, C.; Savitski, M. M.; Huthmacher, C.; Gudgin, E.; Lugo, D.; Beinke, S.; Chapman, T. D.; Roberts, E. J.; Soden, P. E.; Auger, K. R.; Mirguet, O.; Doehner, K.; Delwel, R.; Burnett, A. K.; Jeffrey, P.; Drewes, G.; Lee, K.; Huntly, B. J. P.; Kouzarides, T. Inhibition of Bet Recruitment to Chromatin as An Effective Treatment for Mll-Fusion Leukaemia. *Nature* **2011**, *478*, 529−533.

(22) Delmore, J. E.; Issa, G. C.; Lemieux, M. E.; Rahl, P. B.; Shi, J. W.; Jacobs, H. M.; Kastritis, E.; Gilpatrick, T.; Paranal, R. M.; Qi, J.;

DOI: 10.1021/acs.jcim.5b00265
J. Chem. Inf. Model. 2015, 55, 1926−1935

Chesi, M.; Schinzel, A. C.; Mckeown, M. R.; Heffernan, T. P.; Vakoc, C. R.; Bergsagel, P. L.; Ghobrial, I. M.; Richardson, P. G.; Young, R. A.; Hahn, W. C.; Anderson, K. C.; Kung, A. L.; Bradner, J. E.; Mitsiades, C. S. BET Bromodomain Inhibition as A Therapeutic Strategy to Target C-Myc. *Cell* **2011**, *146*, 904−917.
(23) Filippakopoulos, P.; Qi, J.; Picaud, S.; Shen, Y.; Smith, W. B.; Fedorov, O.; Morse, E. M.; Keates, T.; Hickman, T. T.; Felletar, I.; Philpott, M.; Munro, S.; Mckeown, M. R.; Wang, Y.; Christie, A. L.; West, N.; Cameron, M. J.; Schwartz, B.; Heightman, T. D.; La Thangue, N.; French, C. A.; Wiest, O.; Kung, A. L.; Knapp, S.; Bradner, J. E. Selective Inhibition of BET Bromodomains. *Nature* **2010**, *468*, 1067−1073.
(24) Mertz, J. A.; Conery, A. R.; Bryant, B. M.; Sandy, P.; Balasubramanian, S.; Mele, D. A.; Bergeron, L.; Sims, R. J. Targeting Myc Dependence in Cancer by Inhibiting BET Bromodomains. *Proc. Natl. Acad. Sci. U. S. A.* **2011**, *108*, 16669−16674.
(25) Nicodeme, E.; Jeffrey, K. L.; Schaefer, U.; Beinke, S.; Dewell, S.; Chung, C. W.; Chandwani, R.; Marazzi, I.; Wilson, P.; Coste, H.; White, J.; Kirilovsky, J.; Rice, C. M.; Lora, J. M.; Prinjha, R. K.; Lee, K.; Tarakhovsky, A. Suppression of Inflammation by A Synthetic Histone Mimic. *Nature* **2010**, *468*, 1119−1123.
(26) Steiner, S.; Magno, A.; Huang, D.; Caflisch, A. Does Bromodomain Flexibility Influence Histone Recognition? *FEBS Lett.* **2013**, *587*, 2158−63.
(27) Hornak, V.; Abel, R.; Okur, A.; Strockbine, B.; Roitberg, A.; Simmerling, C. Comparison of Multiple Amber Force Fields and Development of Improved Protein Backbone Parameters. *Proteins: Struct., Funct., Genet.* **2006**, *65*, 712−725.
(28) Wang, J.; Wolf, R. M.; Caldwell, J. W.; Kollman, P. A.; Case, D. A. Development and Testing of A General Amber Force Field. *J. Comput. Chem.* **2004**, *25*, 1157−1174.
(29) Bayly, C. I.; Cieplak, P.; Cornell, W.; Kollman, P. A. A Well-Behaved Electrostatic Potential Based Method Using Charge Restraints for Deriving Atomic Charges The Resp Model. *J. Phys. Chem.* **1993**, *97*, 10269−10280.
(30) Frisch, M. J. T, G. W.; Schlegel, H. B.; Scuseria, G. E.; Robb, M. A.; Cheeseman, J. R.; Scalmani, G.; Barone, V.; Mennucci, B.; Petersson, G. A.; Nakatsuji, H.; Caricato, M.; Li, X.; Hratchian, H. P.; Izmaylov, A. F.; Bloino, J.; Zheng, G.; Sonnenberg, J. L.; Hada, M.; Ehara, M.; Toyota, K.; Fukuda, R.; Hasegawa, J.; Ishida, M.; Nakajima, T.; Honda, Y.; Kitao, O.; Nakai, H.; Vreven, T.; Montgomery, J. A., Jr.; Peralta, J. E.; Ogliaro, F.; Bearpark, M.; Heyd, J. J.; Brothers, E.; Kudin, K. N.; Staroverov, V. N.; Kobayashi, R.; Normand, J.; Raghavachari, K.; Rendell, A.; Burant, J. C.; Iyengar, S. S.; Tomasi, J.; Cossi, M.; Rega, N.; Millam, J. M.; Klene, M.; Knox, J. E.; Cross, J. B.; Bakken, V.; Adamo, C.; Jaramillo, J.; Gomperts, R.; Stratmann, R. E.; Yazyev, O.; Austin, A. J.; Cammi, R.; Pomelli, C.; Ochterski, J. W.; Martin, R. L.; Morokuma, K.; Zakrzewski, V. G.; Voth, G. A.; Salvador, P.; Dannenberg, J. J.; Dapprich, S.; Daniels, A. D.; Farkas, O.; Foresman, J. B.; Ortiz, J. V.; Cioslowski, J.; Fox, D. J. *Gaussian 09*, Gaussian. Inc: Wallingford CT, 2009.
(31) Jorgensen, W. L.; Chandrasekhar, J.; Madura, J. D.; Impey, R. W.; Klein, M. L. Comparison of Simple Potential Functions for Simulating Liquid Water. *J. Chem. Phys.* **1983**, *79*, 926−935.
(32) Case, D. A.; Cheatham, T. E.; Darden, T.; Gohlke, H.; Luo, R.; Merz, K. M.; Onufriev, A.; Simmerling, C.; Wang, B.; Woods, R. J. The Amber Biomolecular Simulation Programs. *J. Comput. Chem.* **2005**, *26*, 1668−1688.
(33) Berendsen, H. J. C.; Postma, J. P. M.; Van Gunsteren, W. F.; Dinola, A.; Haak, J. R. Molecular Dynamics with Coupling to An External Bath. *J. Chem. Phys.* **1984**, *81*, 3684.
(34) Ryckaert, J.-P.; Ciccotti, G.; Berendsen, H. J. C. Numerical Integration of The Cartesian Equations of Motion of A System with Constraints: Molecular Dynamics of N-Alkanes. *J. Comput. Phys.* **1977**, *23*, 327−341.
(35) Vijayaraj, R.; Van Damme, S.; Bultinck, P.; Subramanian, V. Molecular Dynamics and Umbrella Sampling Study of Stabilizing Factors in Cyclic Peptide-Based Nanotubes. *J. Phys. Chem. B* **2012**, *116*, 9922−9933.
(36) Grossfield, A., Wham: An Implementation of The Weighted Histogram Analysis Method, Http://Membrane.Urmc.Rochester.Edu/Content/Wham/, Version2.0.6ed. (accessed June 15, 2014).
(37) Estacio, S. G.; Moreira, R.; Guedes, R. C. Characterizing The Dynamics and Ligand-Specific Interactions in The Human Leukocyte Elastase Through Molecular Dynamics Simulations. *J. Chem. Inf. Model.* **2011**, *51*, 1690−1702.
(38) Amaro, R. E.; Swift, R. V.; Votapka, L.; Li, W. W.; Walker, R. C.; Bush, R. M. Mechanism of 150-Cavity Formation in Influenza Neuraminidase. *Nat. Commun.* **2011**, *2*, 388.
(39) Colombo, G.; Morra, G.; Meli, M.; Verkhivker, G. Understanding Ligand-Based Modulation of The Hsp90 Molecular Chaperone Dynamics at Atomic Resolution. *Proc. Natl. Acad. Sci. U. S. A.* **2008**, *105*, 7976−7981.
(40) Shao, J. Y.; Tanner, S. W.; Thompson, N.; Cheatham, T. E. Clustering Molecular Dynamics Trajectories: 1. Characterizing The Performance of Different Clustering Algorithms. *J. Chem. Theory Comput.* **2007**, *3*, 2312−2334.
(41) Durrant, J. D.; De Oliveira, C. A. F.; Mccammon, J. A. Povme: An Algorithm for Measuring Binding-Pocket Volumes. *J. Mol. Graphics Modell.* **2011**, *29*, 773−776.
(42) *The Pymol Molecular Graphics System*. Version 1.6; Schrödinger Llc: New York, 2013.
(43) Lee, C.; Yang, W.; Parr, R. G. Development of The Colle-Salvetti Correlation-Energy Formula Into A Functional of The Electron Density. *Phys. Rev. B: Condens. Matter Mater. Phys.* **1988**, *37*, 785−789.
(44) Becke, A. D. Density-Functional Exchange-Energy Approximation with Correct Asymptotic Behavior. *Phys. Rev. A: At., Mol., Opt. Phys.* **1988**, *38*, 3098−3100.
(45) Zhang, Y. K. Pseudobond Ab Initio Qm/Mm Approach and Its Applications to Enzyme Reactions. *Theor. Chem. Acc.* **2006**, *116*, 43−50.
(46) Zhang, Y. K. Improved Pseudobonds for Combined Ab Initio Quantum Mechanical/Molecular Mechanical Methods. *J. Chem. Phys.* **2005**, *122*, 024114.
(47) Zhang, Y. K.; Liu, H. Y.; Yang, W. T. Free Energy Calculation on Enzyme Reactions with An Efficient Iterative Procedure to Determine Minimum Energy Paths on A Combined Ab Initio Qm/Mm Potential Energy Surface. *J. Chem. Phys.* **2000**, *112*, 3483−3492.
(48) Zhang, Y. K.; Lee, T. S.; Yang, W. T. A Pseudobond Approach to Combining Quantum Mechanical and Molecular Mechanical Methods. *J. Chem. Phys.* **1999**, *110*, 46−54.
(49) Beeman, D. Some Multistep Methods for Use In Molecular Dynamics Calculations. *J. Comput. Phys.* **1976**, *20*, 130−139.
(50) Shao, Y. M, L. F.; Jung, Y.; Kussmann, J. O. C.; Brown, S. T.; Gilbert, A. T.; Slipchenko, L. V.; Levchenko, S. V.; O'neill, D. P.; Distasio, R. A.; Lochan, R. C.; Wang, T.; Beran, G. J.; Besley, N. A.; Herbert, J. M.; Lin, C. Y.; Van Voorhis, T.; Chien, S. H.; Sodt, A.; Steele, R. P.; Rassolov, V. A.; Maslen, P. E.; Korambath, P. P.; Adamson, R. D.; Austin, B.; Baker, J.; Byrd, E. F.; Dachsel, H.; Doerksen, R. J.; Dreuw, A.; Dunietz, B. D.; Dutoi, A. D.; Furlani, T. R.; Gwaltney, S. R.; Heyden, A.; Hirata, S.; Hsu, C. P.; Kedziora, G.; Khalliulin, R. Z.; Klunzinger, P.; Lee, A. M.; Lee, M. S.; Liang, W.; Lotan, I.; Nair, N.; Peters, B.; Proynov, E. I.; Pieniazek, P. A.; Rhee, Y. M.; Ritchie, J.; Rosta, E.; Sherrill, C. D.; Simmonett, A. C.; Subotnik, J. E.; Woodcock, H. L.; Zhang, W.; Bell, A. T.; Chakraborty, A. K.; Chipman, D. M.; Keil, F. J.; Warshel, A.; Hehre, W. J.; Schaefer, H. F.; Kong, J.; Krylov, A. I.; Gill, P. M.; Head-Gordon, M. *Q-Chem,Version 3.0*,Q-chem,Inc.:Pittsburgh,PA. 2006.
(51) Ponder, J. W.*TINKER,Software Tools for Molecular Design,-Version 4.2*. 2004.
(52) Wu, R. B.; Gong, W. J.; Liu, T.; Zhang, Y. K.; Cao, Z. X. Qm/Mm Molecular Dynamics Study of Purine-Specific Nucleoside Hydrolase. *J. Phys. Chem. B* **2012**, *116*, 1984−1991.
(53) Wu, R. B.; Lu, Z. Y.; Cao, Z. X.; Zhang, Y. K. Zinc Chelation with Hydroxamate in Histone Deacetylases Modulated by Water Access to The Linker Binding Channel. *J. Am. Chem. Soc.* **2011**, *133*, 6110−6113.

DOI: 10.1021/acs.jcim.5b00265
J. Chem. Inf. Model. 2015, 55, 1926−1935

(54) Zhou, J. W.; Xie, H. J.; Liu, Z. H.; Luo, H. B.; Wu, R. B. Structure-Function Analysis of The Conserved Tyrosine and Diverse Pi-Stacking Among Class I Histone Deacetylases: A Qm (Dft)/Mm Md Study. *J. Chem. Inf. Model.* **2014**, *54*, 3162−3171.
(55) Chen, N. H.; Zhou, J. W.; Li, J. B.; Xu, J.; Wu, R. B. Concerted Cyclization of Lanosterol C-Ring and D-Ring Under Human Oxidosqualene Cyclase Catalysis: An Ab Initio Qm/Mm Md Study. *J. Chem. Theory Comput.* **2014**, *10*, 1109−1120.
(56) Brand, M.; Measures, A. M.; Wilson, B. G.; Cortopassi, W. A.; Alexander, R.; Hoss, M.; Hewings, D. S.; Rooney, T. P. C.; Paton, R. S.; Conway, S. J. Small Molecule Inhibitors of Bromodomain-Acetyl-Lysine Interactions. *ACS Chem. Biol.* **2015**, *10*, 22−39.
(57) Picaud, S.; Wells, C.; Felletar, I.; Brotherton, D.; Martin, S.; Savitsky, P.; Diez-Dacal, B.; Philpott, M.; Bountra, C.; Lingard, H.; Fedorov, O.; Muller, S.; Brennan, P. E.; Knapp, S.; Filippakopoulos, P. Rvx-208, An Inhibitor of BET Transcriptional Regulators with Selectivity for The Second Bromodomain. *Proc. Natl. Acad. Sci. U. S. A.* **2013**, *110*, 19754−19759.
(58) Zhang, R.; Monsma, F. Binding Kinetics and Mechanism of Action: Toward The Discovery and Development of Better and Best in Class Drugs. *Expert Opin. Drug Discovery* **2010**, *5*, 1023−1029.
(59) Bai, F.; Xu, Y.; Chen, J.; Liu, Q.; Gu, J.; Wang, X.; Ma, J.; Li, H.; Onuchic, J. N.; Jiang, H. Free Energy Landscape for The Binding Process of Huperzine A to Acetylcholinesterase. *Proc. Natl. Acad. Sci. U. S. A.* **2013**, *110*, 4273−4278.
(60) Kral, A. M.; Ozerova, N.; Close, J.; Jung, J.; Chenard, M.; Fleming, J.; Haines, B. B.; Harrington, P.; Maclean, J.; Miller, T. A.; Secrist, P.; Wang, H.; Heidebrecht, R. J. Divergent Kinetics Differentiate The Mechanism of Action of Two Hdac Inhibitors. *Biochemistry* **2014**, *53*, 725−734.

DOI: 10.1021/acs.jcim.5b00265
J. Chem. Inf. Model. 2015, 55, 1926−1935